

## Photonic bound states in the continuum governed by heating

A. I. Krasnov,<sup>1,2</sup> P. S. Pankin ,<sup>1,2,3,\*</sup> G. A. Romanenko,<sup>4,5</sup> V. S. Sutormin ,<sup>1,2</sup> D. N. Maksimov,<sup>1,2,3</sup>  
S. Ya. Vetrov,<sup>1,2</sup> and I. V. Timofeev<sup>1,2</sup>

<sup>1</sup>*Kirensky Institute of Physics, Federal Research Center KSC SB RAS, Krasnoyarsk 660036, Russia*

<sup>2</sup>*Institute of Engineering Physics and Radio Electronics, Siberian Federal University, Krasnoyarsk 660041, Russia*

<sup>3</sup>*Qingdao Innovation and Development Center, Harbin Engineering University, Qingdao, Shandong 266000, China*

<sup>4</sup>*Department of Physics and Engineering, ITMO University, 197101, Russia*

<sup>5</sup>*Institute of Electronics and Telecommunications, Peter the Great Saint-Petersburg Polytechnic University, Saint-Petersburg 195251, Russia*



(Received 6 July 2023; revised 29 November 2023; accepted 4 April 2024; published 10 May 2024)

A photonic crystal microcavity with the liquid crystal resonant layer tunable by heating has been implemented. The multiple vanishing resonant lines corresponding to optical bound states in the continuum are observed. The abrupt change in the resonant linewidth near the vanishing point can be used for temperature sensing.

DOI: [10.1103/PhysRevE.109.054703](https://doi.org/10.1103/PhysRevE.109.054703)

### I. INTRODUCTION

One-dimensional (1D) photonic crystal (PhC) is a periodic structure formed by layers with different refractive indices (RIs) [1]. The optical thicknesses of the alternating layers are comparable with the wavelength, which leads to the Bragg diffraction of light. In the photonic band gap (PBG) spectral region the PhC reflects light with small losses. The resonant layer embedded between two PhC mirrors forms a microcavity, which supports microcavity (MC) modes [2].

When the resonant layer is an anisotropic material the MC mode can be transformed into a bound state in the continuum (BIC) [3–7]. The BIC is a nonradiative localized eigenmode embedded in the continuum of propagating waves [8]. The BIC is a general wave phenomenon, which occurs in quantum mechanics, radio physics, photonics, and acoustics [8–12]. Variation of parameters of the system near the BIC affects the coupling between the localized mode and the continuum of propagating waves and thereby tunes the radiation decay rate. The BIC has been used in various applications, such as lasers [13–15], waveguides [16–20], nanocavities [21,22], amplified chiral response [23,24], nonlinear thermo-optical response [25,26], trapping and sorting of nanoparticles [27], perfect absorbers [28,29], etc. Due to the narrow spectral line the quasi-BICs have been used for RI sensing [30–33], mechanical pressure sensing [34], as well as for temperature sensing [35,36]. In this work, we demonstrate an optical BIC in a PhC microcavity tunable by heating the anisotropic liquid crystal (LC) resonant layer having in mind potential applications for temperature sensing. In contrast to the conventional approach based on the shift of the MC mode spectral line position [37,38], we suggest a sensor based on the temperature change in the resonant linewidth.

### II. MODEL

The microcavity consists of a LC layer embedded between two identical 1D PhCs, see Fig. 1(a). The silicon nitride ( $\text{Si}_3\text{N}_4$ ) and silicon dioxide ( $\text{SiO}_2$ ) layers are deposited on glass substrate by using the plasma enhanced chemical vapor deposition method. The number of periods in PhC is eight plus one unpaired layer of silicon nitride. Polyvinyl alcohol (PVA) layers are formed on each PhC by the spin-coating method and then mechanically rubbed to ensure a homogeneous planar alignment of the LC. The gap between PhC mirrors is provided with Teflon spacers. The 4-pentyl-4'-cyanobiphenyl (5CB) nematic LC is embedded into the gap by the capillary method.

The thicknesses and RIs of all layers are presented in Table I. In nematic LCs the optical axis (OA) coincides with the preferred alignment of the long axes of the LC molecules, which is described by the unit vector  $\mathbf{a} = [\cos(\phi), \sin(\phi), 0]$ , called the director, see Fig. 1(b) [39].

The polarizing microscopy images of the optical texture of the LC layer confirm the planar LC alignment, see Fig. 1(c). The uniform dark texture is observed when rubbing directions of PVA layers are parallel to the polarizer or the analyzer, while the maximum intensity of the transmitted light is observed upon rotation of the crossed polarizers by  $45^\circ$ . The microcavity is conjugated with glass hemispherical lenses with RI  $n_G = 1.5$ . The immersion oil with RI of 1.5 is placed between the glass substrates and lenses to eliminate the air gap.

The experimental setup for measuring the microcavity transmittance spectra is shown in Fig. 1(d). The incoherent radiation from the source propagates through an optical fiber and a polarizer. After passing through the polarizer, the TE-polarized (TE wave) or TM-polarized (TM wave) radiation is focused on the microcavity. The outgoing radiation is collected in a fiber optic collimator connected to the spectrometer. The microcavity is heated using the thermostat with temperature controlling by a thermistor. The azimuthal angle

\*pavel-s-pankin@iph.krasn.ru

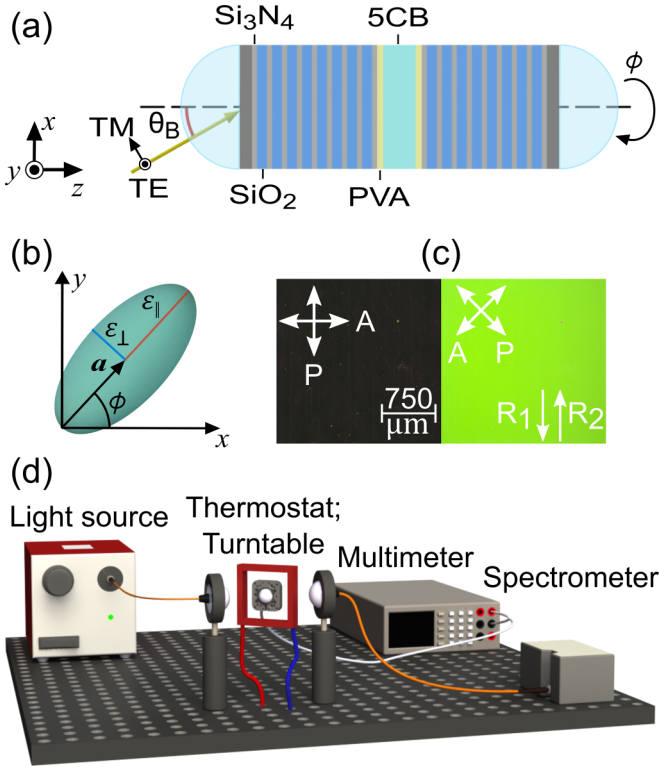


FIG. 1. (a) The microcavity model. (b) The orientation of the LC permittivity ellipsoid. (c) Polarizing optical microscope images of the LC layer texture taken in crossed polarizers.  $R_1$  and  $R_2$  are the PVA rubbing directions. Crossed double arrows show the direction of the polarizer (P) and analyzer (A). (d) The experimental setup.

$\phi$  of the LC OA orientation is changed by rotation of the sample on the motorized turntable.

### III. RESULTS AND DISCUSSION

Figure 2(a) shows the measured PhC transmittance spectra for TE and TM waves incident at angle  $\theta_B = \text{asin}\{(n_{\text{Si}_3\text{N}_4}/n_G) \sin[\text{atan}(n_{\text{SiO}_2}/n_{\text{Si}_3\text{N}_4})]\} \approx 53^\circ$ . The wide dip corresponding to the PBG for TE waves is observed, while TM waves pass through the PhC due to the Brewster effect at the  $\text{Si}_3\text{N}_4$ - $\text{SiO}_2$  interfaces [40]. The TE-polarized spectrum demonstrates resonant transmittance at  $\lambda = 723$  nm corresponding to edge mode excitation [1]. The transmittance spectra of the microcavity for different values of the azimuthal angle  $\phi$  at room temperature are shown in Figs. 2(b)–2(f). The oscillating behavior of the envelope of the transmittance spectra can be seen. It can be explained by the fact that PhC

TABLE I. Parameters of the layers.

Layer	Thickness ( $\mu\text{m}$ )	Refractive index at $\lambda = 570$ nm
$\text{Si}_3\text{N}_4$	0.08	2.15
$\text{SiO}_2$	0.153	1.45
PVA	0.1	1.48
5CB	10.03	$n_\perp = \sqrt{\epsilon_\perp} = 1.55$ $n_\parallel = \sqrt{\epsilon_\parallel} = 1.74$

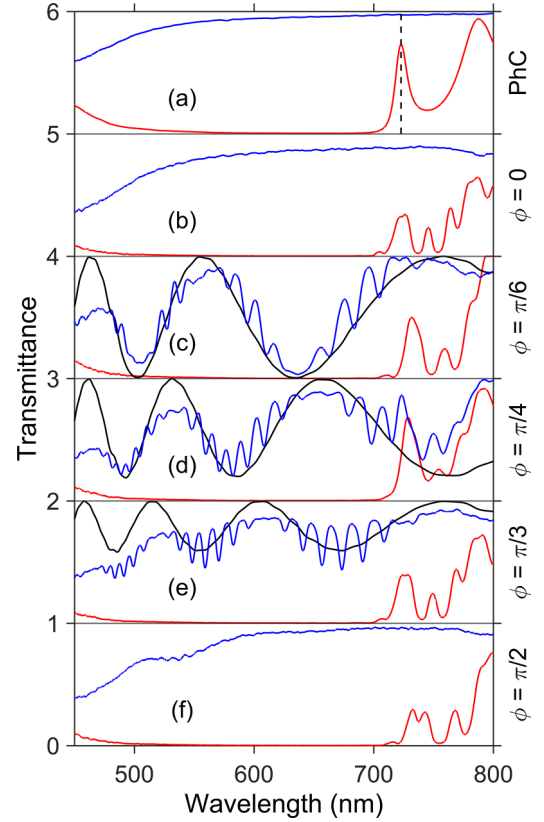


FIG. 2. Measured transmittance spectra for the TE (red line) and TM (blue line) waves at the Brewster's angle. The spectra of (a) PhC and (b)–(f) microcavity at different values  $\phi$ . The vertical dashed line in (a) corresponds to the edge mode. The black lines in (c)–(e) show the TM-polarized transmittance spectra of the LC layer in the parallel polarizers scheme.

transmits only TM-polarized light. Thus, the problem can be treated as transmission through the anisotropic LC layer in the parallel polarizers scheme. To confirm this statement the additional calculations for LC layer in parallel polarizers scheme are presented in Figs. 2(c)–2(e). The initial linear TM-polarization state changes due to the propagation through the LC layer [39]. The zero transmittance corresponds to the case when the LC layer is equivalent to the half-wave phase plate, see Fig. 2(c). In the PBG spectral range the multiple resonant dips corresponding to the MC modes are observed at the envelope line when  $\phi \neq 0, \pi/2$ , see Figs. 2(c)–2(e). The position of the dips, at the rough estimation, corresponds to the integer multiple of half-wavelengths LC optical thickness condition [40]. More strictly, the position of the resonant wavelengths can be obtained through the solution of the eigenfrequency problem, see Fig. 4(e). It can be seen that the position and width of the resonant lines are strongly dependent on the value  $\phi$ . The width of the resonant line is determined by the total decay rate  $\gamma_{\text{tot}} = \gamma + \gamma_0$ , which is the sum of the radiation decay rate  $\gamma$  into the TM polarized continuum and the material loss rate  $\gamma_0$ . The cases  $\phi = 0, \pi/2$  correspond to symmetry-protected BICs with zero radiation decay rate  $\gamma = 0$ , due to the orthogonality of the localized TE and propagating TM waves [4,7]. The resonant dips do not occur in the corresponding spectra, see Figs. 2(b) and 2(f).

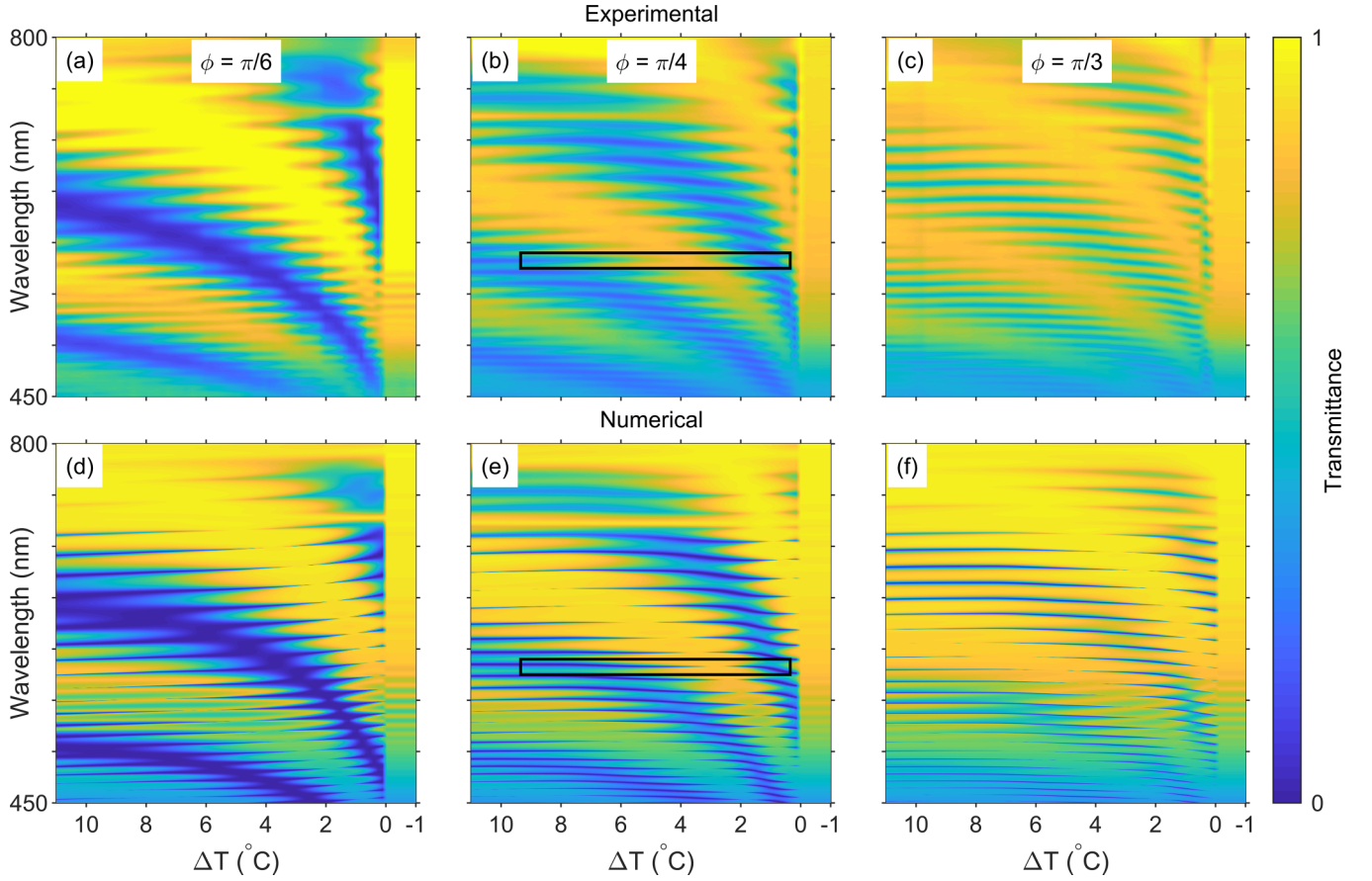


FIG. 3. The (a)–(c) measured and (d)–(f) calculated dependencies of the microcavity transmittance spectra on the difference  $\Delta T = T_c - T$  between the temperature  $T$  of the LC layer and the temperature of the LC and isotropic liquid phase transition  $T_c \approx 35^\circ\text{C}$ . The black rectangle areas in (b) and (e) are scaled up in Fig. 4(a) and Fig. 4(c), respectively.

The measured temperature transformation of the microcavity spectra for fixed values  $\phi = \pi/6, \pi/4, \pi/3$  is shown in Figs. 3(a)–3(c). It can be seen that position and width of the resonant lines change when temperature  $T$  increases from  $24^\circ\text{C}$  to  $35^\circ\text{C}$ . The radiation decay rate  $\gamma$  is determined by the Poynting vector of TM waves of the resonant mode  $\gamma \propto |E_x|^2$  at the LC-PVA boundary [3]. The value  $E_x$  is a sum of the ordinary (o-wave) and extraordinary (e-wave) waves  $E_x = E_{ox} + E_{ex}$ . The polarization vectors  $\mathbf{E}_{o,e}$  of the o- and e-waves are determined by the direction of the LC OA  $\mathbf{a}$ , the permittivities of the o- and e-waves  $\varepsilon_{o,e}(T)$ , and the unit vectors in the propagation directions  $\boldsymbol{\kappa}_{o,e}(T) = [\kappa_{o,ex}; 0; \kappa_{o,e,z}]$ . According to Ref. [41] one can write

$$\begin{aligned} \mathbf{E}_o &= E_o [\mathbf{a} \times \boldsymbol{\kappa}_o], \\ \mathbf{E}_e &= E_e \left[ \mathbf{a} - \frac{\varepsilon_e(\alpha)}{\varepsilon_o} \boldsymbol{\kappa}_e(\boldsymbol{\kappa}_e \mathbf{a}) \right], \end{aligned} \quad (1)$$

where  $\alpha$  is the angle between the vectors  $\mathbf{a}$  and  $\boldsymbol{\kappa}_e$ .

The thermal motion of the LC molecules leads to a change in the permittivities  $\varepsilon_o = \varepsilon_\perp(T)$  and  $\varepsilon_\perp(T) \leq \varepsilon_e(\alpha) \leq \varepsilon_\parallel(T)$ . For certain values of temperature  $T$  the condition  $E_x = E_{ox} + E_{ex} = 0$  can be satisfied. The radiation decay rate  $\gamma$  in this

case is equal to zero  $\gamma = 0$ , and the resonant line collapses. This case corresponds to Friedrich-Wintgen BIC [42], also called accidental BIC [16] or parametric BIC [10]. The temperature changing in the LC permittivities leads to the spectral shift of the resonant wavelengths, due to the changing of the LC layer optical thickness. At temperature  $T_c = 35^\circ\text{C}$  the phase transition of the LC to the isotropic liquid is observed. The TE and TM waves are not mixed, and resonant lines vanish [6].

Figures 3(d)–3(f) present temperature transformation of the microcavity spectra calculated by the Berreman transfer matrix method [43]. For calculation of spectra the frequency-dependent [44–48] and temperature-dependent refractive indices [49] were adjusted within 5% to provide agreement with the experiment. In Fig. 4(a) we demonstrate the transmittance in the vicinity of the BIC shown in Fig. 3(b) by black rectangle. In Fig. 4(b) we show the temperature dependence of the resonant linewidth and its temperature derivative. In Fig. 4(b) one can see that at the BIC temperature  $T$  the derivative exhibits an abrupt change. In Fig. 4(c) we show the numerical data obtained by the Berreman method in the same range of parameters.

In the framework of the temporal coupled-mode theory (TCMT) [50] the LC layer and the PhCs are considered as a

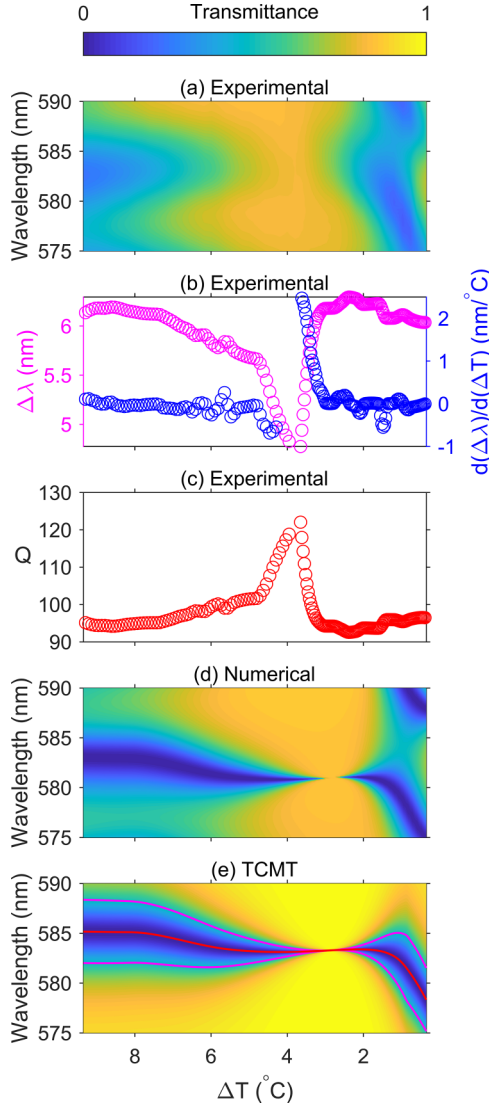


FIG. 4. (a) The measured, (d) calculated by Berreman's method, and (e) using TCMT model dependences of the microcavity transmittance spectra on the difference  $\Delta T = T_c - T$  between the temperature  $T$  of the LC layer and the temperature of the LC and isotropic liquid phase transition  $T_c \approx 35^\circ\text{C}$ . (e) shows  $2\pi/\omega_0$  (red line);  $2\pi/(\omega_0 \pm \gamma_{tot})$  (magenta line). The linewidth  $\Delta\lambda$  (b), its derivative  $d(\Delta\lambda)/d(\Delta T)$  (b), and  $Q$  factor (c) for the resonant line.

resonator and waveguides. The amplitude  $a$  of the MC mode obeys the following equations:

$$\frac{da}{dt} = -(i\omega_0 + \gamma + \gamma_0)a + \langle d^* | \begin{pmatrix} s_1^{(+)} \\ s_2^{(+)} \end{pmatrix}, \quad (2)$$

$$\begin{pmatrix} s_1^{(-)} \\ s_2^{(-)} \end{pmatrix} = \widehat{C} \begin{pmatrix} s_1^{(+)} \\ s_2^{(+)} \end{pmatrix} + a|d\rangle. \quad (3)$$

Here  $\omega_0$  is the resonant frequency,  $|d\rangle$  is the column vector of coupling constants,  $s_{1,2}^{(\pm)}$  are amplitudes of TM waves in the PhC waveguides. In the case of central-plane mirror symmetry, the nonresonant scattering matrix  $\widehat{C}$  at the BIC frequency is written as

$$\widehat{C} = e^{i\psi} \begin{pmatrix} \rho & \pm i\tau \\ \pm i\tau & \rho \end{pmatrix}, \quad (4)$$

where  $\psi$  and  $\rho$  are the phase and amplitude of the complex reflection coefficient,  $\tau$  is the amplitude of the complex transmission coefficient,  $\rho^2 + \tau^2 = 1$ . The coupling constant vector for the case when the MC mode is even with respect to the mirror plane is written as

$$|d\rangle = \begin{pmatrix} d_1 \\ d_2 \end{pmatrix} = e^{i\frac{\psi}{2}} \sqrt{\frac{\gamma}{2(1+\rho)}} \begin{pmatrix} \pm\tau - i(1+\rho) \\ \pm\tau - i(1+\rho) \end{pmatrix}, \quad (5)$$

and for the case of odd MC mode it is written as

$$|d\rangle = \begin{pmatrix} d_1 \\ d_2 \end{pmatrix} = e^{i\frac{\psi}{2}} \sqrt{\frac{\gamma}{2(1+\rho)}} \begin{pmatrix} \pm\tau + i(1+\rho) \\ \mp\tau - i(1+\rho) \end{pmatrix}. \quad (6)$$

Assuming that harmonic waves  $s^{(\pm)} \propto e^{-i\omega t}$  propagate in the waveguides, the Eqs. (2) and (3) yield the final expression for the scattering matrix  $\widehat{S}$  in following form:

$$\widehat{S}(T, \omega) = \widehat{C} + \frac{|d\rangle\langle d^*|}{i[\omega_0(T) - \omega] + \gamma(T) + \gamma_0}. \quad (7)$$

The complex eigenfrequency in dependence on temperature  $\omega_r(T) = \omega_0(T) - i\gamma(T)$  was found analytically by solving the eigenvalue problem for an open system, see Supplemental in Ref. [4]. The major contribution to the material loss in the fabricated microcavity is due to the conducting transparent layers of aluminum-doped zinc oxide deposited on the glass substrates. It cannot be taken into account by solving the eigenvalue problem formulated for the semi-infinite PhCs, therefore the rate of material loss  $\gamma_0$  is fitted to be consistent with the numerical spectra. In Fig. 4(d) we demonstrate the TCMT solution with fitted  $\gamma_0$ . One can see a good agreement between Figs. 4(d) and 4(c). Although the presence of the conducting layers decrease the maximum possible quality factor  $Q = \omega_0/2\gamma_{tot}$  to the value  $Q_{max} = \omega_0/2\gamma_0$  at the BIC frequency, it ensures the voltage-tunable  $Q$  factor, which has been demonstrated in Ref. [7].

#### IV. CONCLUSION

In this work we demonstrated an optical bound state in the continuum in a photonic crystal microcavity tunable by heating the anisotropic liquid crystal resonant layer. We experimentally measured the temperature dependencies of the transmittance spectrum at Brewster's angle and observed multiple vanishing resonant lines, which indicate the occurrence of optical bound states in the continuum. The obtained dependencies are explained theoretically with application of the temporal coupled mode theory and rigorous Berreman's transfer matrix method. It is found that in the point of optical bound state in the continuum the resonant linewidth has an abrupt change, which can be employed for engineering temperature sensors.

The data that support the findings of this study are available from the corresponding author, P.S.P., upon reasonable request.

#### ACKNOWLEDGMENTS

This work was supported by the Russian Science Foundation under Grant No. 22-22-00687. The authors would

like to express their special gratitude to the Krasnoyarsk Regional Center for Collective Use of the Federal Research Center “Krasnoyarsk Scientific Center, Siberian Branch of the

Russian Academy of Sciences” for providing equipment within this project.

The authors declare no conflicts of interest.

- [1] J. D. Joannopoulos, S. G. Johnson, J. N. Winn, and R. D. Meade, *Photonic Crystals: Molding the Flow of Light*, 2nd ed. (Princeton University Press, Princeton, 2008), p. 304.
- [2] A. V. Kavokin, J. J. Baumberg, G. Malpuech, and F. P. Laussy, *Microcavities* (Oxford University Press, Oxford, 2017), Vol. 21.
- [3] I. V. Timofeev, D. N. Maksimov, and A. F. Sadreev, Optical defect mode with tunable Q factor in a one-dimensional anisotropic photonic crystal, *Phys. Rev. B* **97**, 024306 (2018).
- [4] P. S. Pankin, B.-R. Wu, J.-H. Yang, K.-P. Chen, I. V. Timofeev, and A. F. Sadreev, One-dimensional photonic bound states in the continuum, *Commun. Phys.* **3**, 91 (2020).
- [5] D. O. Ignatyeva and V. I. Belotelov, Bound states in the continuum enable modulation of light intensity in the Faraday configuration, *Opt. Lett.* **45**, 6422 (2020).
- [6] B.-R. Wu, J.-H. Yang, P. S. Pankin, C. Huang, W. Lee, D. N. Maksimov, I. V. Timofeev, and K.-P. Chen, Quasi-bound states in the continuum with temperature-tunable Q factors and critical coupling point at Brewster’s angle, *Laser Photon. Rev.* **15**, 2000290 (2021).
- [7] A. I. Krasnov, P. S. Pankin, D. S. Buzin, G. A. Romanenko, V. S. Sutormin, F. V. Zelenov, A. N. Masyugin, M. N. Volochaev, S. Y. Vetrov, and I. V. Timofeev, Voltage-tunable Q factor in a photonic crystal microcavity, *Opt. Lett.* **48**, 1666 (2023).
- [8] C. W. Hsu, B. Zhen, A. D. Stone, J. D. Joannopoulos, and M. Soljačić, Bound states in the continuum, *Nature Rev. Mater.* **1**, 16048 (2016).
- [9] A. F. Sadreev, Interference traps waves in open system: Bound states in the continuum, *Rep. Prog. Phys.* **84**, 055901 (2021).
- [10] K. L. Koshelev, Z. F. Sadrieva, A. A. Shcherbakov, Y. S. Kivshar, and A. A. Bogdanov, Bound states in the continuum in photonic structures, *Phys. Usp.* **66**, 494 (2023).
- [11] S. I. Azzam and A. V. Kildishev, Photonic bound states in the continuum: From basics to applications, *Adv. Opt. Mater.* **9**, 2001469 (2021).
- [12] S. Joseph, S. Pandey, S. Sarkar, and J. Joseph, Bound states in the continuum in resonant nanostructures: an overview of engineered materials for tailored applications, *Nanophoton.* **10**, 4175 (2021).
- [13] A. Kodigala, T. Lepetit, Q. Gu, B. Bahari, Y. Fainman, and B. Kanté, Lasing action from photonic bound states in continuum, *Nature (London)* **541**, 196 (2017).
- [14] C. Huang, C. Zhang, S. Xiao, Y. Wang, Y. Fan, Y. Liu, N. Zhang, G. Qu, H. Ji, J. Han, L. Ge, Y. Kivshar, and Q. Song, Ultrafast control of vortex microlasers, *Science* **367**, 1018 (2020).
- [15] J. Yang, Z. Huang, D. N. Maksimov, P. S. Pankin, I. V. Timofeev, K. Hong, H. Li, J. Chen, C. Hsu, Y. Liu, T. Lu, T. Lin, C. Yang, and K. Chen, Low-Threshold Bound State in the Continuum Lasers in Hybrid Lattice Resonance Metasurfaces, *Laser Photon. Rev.* **15**, 2100118 (2021).
- [16] C. W. Hsu, B. Zhen, J. Lee, S. L. Chua, S. G. Johnson, J. D. Joannopoulos, and M. Soljačić, Observation of trapped light within the radiation continuum., *Nature (London)* **499**, 188 (2013).
- [17] E. A. Bezus, D. A. Bykov, and L. L. Doskolovich, Bound states in the continuum and high-Q resonances supported by a dielectric ridge on a slab waveguide, *Photon. Res.* **6**, 1084 (2018).
- [18] J. Gomis-Bresco, D. Artigas, and L. Torner, Anisotropy-induced photonic bound states in the continuum, *Nature Photon.* **11**, 232 (2017).
- [19] S. Mukherjee, J. Gomis-Bresco, D. Artigas, and L. Torner, Unidirectional guided resonances in anisotropic waveguides, *Opt. Lett.* **46**, 2545 (2021).
- [20] E. Bulgakov, A. Pilipchuk, and A. Sadreev, Desktop laboratory of bound states in the continuum in metallic waveguide with dielectric cavities, *Phys. Rev. B* **106**, 075304 (2022).
- [21] M. V. Rybin, K. L. Koshelev, Z. F. Sadrieva, K. B. Samusev, A. A. Bogdanov, M. F. Limonov, and Y. S. Kivshar, High-Q supercavity modes in subwavelength dielectric resonators, *Phys. Rev. Lett.* **119**, 243901 (2017).
- [22] K. Koshelev, S. Kruk, E. Melik-Gaykazyan, J.-H. Choi, A. Bogdanov, H.-G. Park, and Y. Kivshar, Subwavelength dielectric resonators for nonlinear nanophotonics, *Science* **367**, 288 (2020).
- [23] T. Shi, Z.-L. Deng, G. Geng, X. Zeng, Y. Zeng, G. Hu, A. Overvig, J. Li, C.-W. Qiu, A. Alù, Y. S. Kivshar, and X. Li, Planar chiral metasurfaces with maximal and tunable chiroptical response driven by bound states in the continuum, *Nature Commun.* **13**, 4111 (2022).
- [24] M. V. Gorkunov, A. A. Antonov, and Y. S. Kivshar, Metasurfaces with maximum chirality empowered by bound states in the continuum, *Phys. Rev. Lett.* **125**, 093903 (2020).
- [25] D. N. Maksimov, A. S. Kostyukov, A. E. Ershov, M. S. Molochev, E. N. Bulgakov, and V. S. Gerasimov, Thermo-optic hysteresis with bound states in the continuum, *Phys. Rev. A* **106**, 063507 (2022).
- [26] A. Barulin, O. Pashina, D. Riabov, O. Sergaeva, Z. Sadrieva, A. Shcherbakov, V. Rutckaia, J. Schilling, A. Bogdanov, I. Sinev *et al.*, Thermo-optical bistability enabled by bound states in the continuum in silicon metasurfaces, [arXiv:2308.05399](https://arxiv.org/abs/2308.05399).
- [27] E. N. Bulgakov and A. F. Sadreev, Self-trapping of nanoparticles by bound states in the continuum, *Phys. Rev. B* **106**, 165430 (2022).
- [28] Z. Wang, Y. Liang, J. Qu, M. K. Chen, M. Cui, Z. Cheng, J. Zhang, J. Yao, S. Chen, D. P. Tsai *et al.*, Plasmonic bound states in the continuum for unpolarized weak spatially coherent light, *Photon. Res.* **11**, 260 (2023).
- [29] R. G. Bikbaev, D. N. Maksimov, P. S. Pankin, M.-J. Ye, K.-P. Chen, and I. V. Timofeev, Enhanced light absorption in tamm metasurface with a bound state in the continuum, *Photonics Nanostruct. Fundam. Appl.* **55**, 101148 (2023).
- [30] S. Romano, M. Mangini, E. Penzo, S. Cabrini, A. C. De Luca, I. Rendina, V. Mocella, and G. Zito, Ultrasensitive surface refractive index imaging based on quasi-bound states in the continuum, *ACS Nano* **14**, 15417 (2020).

- [31] D. N. Maksimov, V. S. Gerasimov, S. Romano, and S. P. Polyutov, Refractive index sensing with optical bound states in the continuum, *Opt. Express* **28**, 38907 (2020).
- [32] A. M. Chernyak, M. G. Barsukova, A. S. Shorokhov, A. I. Musorin, and A. A. Fedyanin, Bound states in the continuum in magnetophotonic metasurfaces, *JETP Lett.* **111**, 46 (2020).
- [33] C. Schiattarella, G. Sanità, B. G. Alulema, V. Lanzio, S. Cabrini, A. Lamberti, I. Rendina, V. Mocella, G. Zito, and S. Romano, High-Q photonic aptasensor based on avoided crossing bound states in the continuum and trace detection of ochratoxin A, *Biosens. Bioelec. X* **12**, 100262 (2022).
- [34] A. Sadreev, E. Bulgakov, A. Pilipchuk, A. Miroschnichenko, and L. Huang, Degenerate bound states in the continuum in square and triangular open acoustic resonators, *Phys. Rev. B* **106**, 085404 (2022).
- [35] F. Wu, J. Wu, Z. Guo, H. Jiang, Y. Sun, Y. Li, J. Ren, and H. Chen, Giant enhancement of the Goos-Hanchen shift assisted by quasibound states in the continuum, *Phys. Rev. Appl.* **12**, 014028 (2019).
- [36] I. Yusupov, D. Filonov, A. Bogdanov, P. Ginzburg, M. V. Rybin, and A. Slobozhanyuk, Chipless wireless temperature sensor based on quasi-BIC resonance, *Appl. Phys. Lett.* **119**, 193504 (2021).
- [37] V. G. Arkhipkin, V. A. Gunyakov, S. A. Myslivets, V. P. Gerasimov, V. Y. Zyryanov, S. Y. Vetrov, and V. F. Shabanov, One-dimensional photonic crystals with a planar oriented nematic layer: Temperature and angular dependence of the spectra of defect modes, *J. Exp. Theor. Phys.* **106**, 388 (2008).
- [38] Y.-C. Yang, C.-S. Kee, J.-E. Kim, H. Y. Park, J.-C. Lee, and Y.-J. Jeon, Photonic defect modes of cholesteric liquid crystals, *Phys. Rev. E* **60**, 6852 (1999).
- [39] L. M. Blinov, *Structure and Properties of Liquid Crystals*, Topics in applied physics (Springer, Dordrecht, Berlin, 2010), p. 458.
- [40] S. A. Akhmanov and S. Y. Nikitin, *Physical Optics* (Clarendon Press, Oxford, 1997).
- [41] F. V. Ignatovich and V. K. Ignatovich, Optics of anisotropic media, *Uspekhi Fiz. Nauk* **182**, 759 (2012).
- [42] H. Friedrich and D. Wintgen, Interfering resonances and bound states in the continuum, *Phys. Rev. A* **32**, 3231 (1985).
- [43] D. W. Berreman, Optics in stratified and anisotropic media:  $4 \times 4$ -matrix formulation, *J. Opt. Soc. Am.* **62**, 502 (1972).
- [44] K. Luke, Y. Okawachi, M. R. E. Lamont, A. L. Gaeta, and M. Lipson, Broadband mid-infrared frequency comb generation in a  $\text{Si}_3\text{N}_4$  microresonator, *Opt. Lett.* **40**, 4823 (2015).
- [45] L. Gao, F. Lemarchand, and M. Lequime, Refractive index determination of  $\text{SiO}_2$  layer in the UV/Vis/NIR range: spectrophotometric reverse engineering on single and bi-layer designs, *J. Eur. Opt. Soc.-Rapid Publ.* **8** (2013).
- [46] M. J. Schnepf, M. Mayer, C. Kuttner, M. Tebbe, D. Wolf, M. Dulle, T. Altantzis, P. Formanek, S. Förster, S. Bals, T. A. F. König, and A. Fery, Nanorattles with tailored electric field enhancement, *Nanoscale* **9**, 9376 (2017).
- [47] I. A. Tambasov, M. N. Volochev, A. S. Voronin, N. P. Evsevskaya, A. N. Masyugin, A. S. Aleksandrovskii, T. E. Smolyarova, I. V. Nemtsev, S. A. Lyashchenko, G. N. Bondarenko, and E. V. Tambasova, Structural, optical, and thermoelectric properties of the ZnO: Al films synthesized by atomic layer deposition, *Physica Solid State* **61**, 1904 (2019).
- [48] S.-T. Wu, C. Wu, M. Warenaugh, and M. Ismaili, Refractive index dispersions of liquid crystals, *Opt. Eng.* **32**, 1775 (1993).
- [49] M. S. Sefton, A. R. Bowdler, and H. J. Coles, Light scattering studies of the viscoelastic ratios of mixtures of side chain liquid crystalline polymers in low molar mass mesogens, *Mol. Cryst. Liq. Cryst.* **129**, 1 (1985).
- [50] S. Fan, W. Suh, and J. D. Joannopoulos, Temporal coupled-mode theory for the Fano resonance in optical resonators, *J. Opt. Soc. Am. A* **20**, 569 (2003).